

Direct Bandgap Light Emission from Strained Germanium Nanowires Coupled with High-Q Nanophotonic Cavities

Jan Petykiewicz,[†] Donguk Nam,^{*,‡} David S. Sukhdeo,[†] Shashank Gupta,[†] Sonia Buckley,[†] Alexander Y. Piggott,[†] Jelena Vučković,^{*,†} and Krishna C. Saraswat^{*,†}

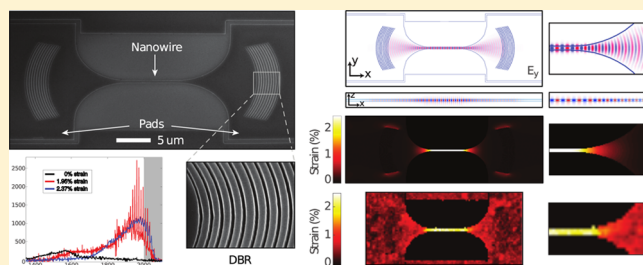
[†]Department of Electrical Engineering, Stanford University, Stanford, California 94305, United States

[‡]Department of Electronic Engineering, Inha University, Incheon 402-751, South Korea

S Supporting Information

ABSTRACT: A silicon-compatible light source is the final missing piece for completing high-speed, low-power on-chip optical interconnects. In this paper, we present a germanium nanowire light emitter that encompasses all the aspects of potential low-threshold lasers: highly strained germanium gain medium, strain-induced pseudoheterostructure, and high-Q nanophotonic cavity. Our nanowire structure presents greatly enhanced photoluminescence into cavity modes with measured quality factors of up to 2000. By varying the dimensions of the germanium nanowire, we tune the emission wavelength over more than 400 nm with a single lithography step. We find reduced optical loss in optical cavities formed with germanium under high (>2.3%) tensile strain. Our compact, high-strain cavities open up new possibilities for low-threshold germanium-based lasers for on-chip optical interconnects.

KEYWORDS: Germanium, strain, group IV, nanophotonics, optical interconnects, pseudoheterostructure



A group IV light source is the long-standing holy grail of integrated photonics, promising to enable monolithic integration of silicon (Si) CMOS electronics with high-speed and low-power optical systems.^{1–4} Previously demonstrated Si-compatible sources have included emission from Si nanowires,⁵ Si Raman lasers,^{6,7} as well as germanium (Ge)^{8,9} and germanium–tin (GeSn)¹⁰ lasers. Of these sources, Ge and GeSn offer the prospect of electrically pumped lasers, a crucial component of a fully integrated optoelectronic system.

Both optically and electrically pumped Ge lasers have been reported in the literature,^{8,9,11} using a combination of 0.2% tensile strain and heavy n-type doping to achieve optical gain.¹² However, the high thresholds (30 kW/cm², 280 kA/cm²) and very large sizes of these lasers make them impractical for most on-chip applications. In addition, a recent report contradicts these findings,¹³ noting that the pump-induced absorption in 0.2% strained Ge is too high to permit lasing at the reported pump powers, indicating that it is imperative to reduce the lasing threshold. More recently, a GeSn laser was demonstrated;¹⁰ however, it also suffered from similarly high threshold power (325 kW/cm²) and only operated at cryogenic temperatures (<90 K).

Mechanical tensile strain can address the problems of both Ge and GeSn lasers by altering the bandstructure and increasing the electron population in the direct valley and thus the optical gain.^{14–17} Theoretical modeling predicts that applying 2% biaxial tensile strain to Ge can reduce the lasing threshold by 200× compared to the reported Ge lasers.¹⁸ Similarly, applying the same amount of tensile strain can reduce

the threshold of a GeSn laser with 5% tin content by almost 2 orders of magnitude.¹⁹ The reported Ge lasers exhibited only very slight (~0.2%) strains^{8,9} and could at best provide a ~3× reduction in threshold relative to unstrained Ge.^{16,18} Devices with higher tensile strains have been successfully demonstrated,^{20–22} but either did not include optical cavities or had optical cavities with low quality (Q) factors.^{21,23,24} Similarly, carrier confinement in a double-heterostructure has been explored as an avenue for achieving lasing, but requires complex material growth and is often incompatible with tensile strain.^{25,26}

In this work, we propose a novel structure that addresses all three issues jointly: high tensile strain for improved material gain, a compact and high-Q optical nanocavity, and a pseudoheterostructure. We present a new nanocavity design capable of confining both light and excited carriers in a >2.3% tensile-strained active region while maintaining quality factors up to 2000, making radiative losses negligible toward the net gain in our devices. The amount of tensile strain can be conveniently tuned by varying the nanowire geometry as first demonstrated by Minamisawa et al.,²⁷ enabling tunable emission over a wavelength range of more than 400 nm with a fabrication process which requires only a single lithography step. We envision that our compact optical resonator with

Received: September 30, 2015

Revised: February 21, 2016

highly strained Ge nanowire gain medium will pave the way toward practical integrated light sources for optical interconnects.

Figure 1a presents a scanning electron micrograph (SEM) of a fabricated device, consisting of an 8 μm long highly strained

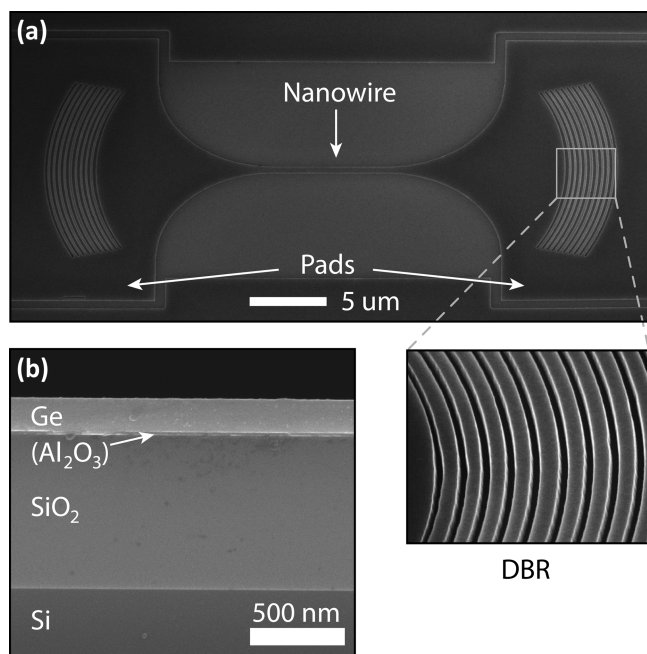


Figure 1. Strained Ge nanowire. (a) Scanning electron micrograph (SEM) of a fabricated device, showing the etched Ge nanowire and adjacent distributed Bragg-reflector (DBR) mirrors (detail view). (b) Side-view SEM of the initial Ge-on-insulator material stack.

Ge nanowire surrounded by two large pads containing distributed Bragg reflector (DBR) mirrors which form the optical cavity. The device is fabricated in a material stack consisting of four layers: 200 nm Ge, 25 nm Al_2O_3 , 850 nm SiO_2 , and Si wafer (Figure 1b). Fabrication details for creating the material stack are provided in the Supporting Information (SI). The Ge layer is n-type doped with $1 \times 10^{19} \text{ cm}^{-3}$ phosphorus atoms using in situ doping during growth. The device is patterned using a single electron beam lithography

step, followed by a HBr/Cl_2 dry etch for pattern transfer to the Ge layer. The structure is then undercut by a KOH wet etch to selectively remove the Al_2O_3 layer, releasing the very slightly (0.2%) strained Ge layer from the substrate. This step allows the large pads to contract, amplifying the strain in the nanowire.^{20,28,29}

While crucial for inducing strain in the nanowire, the undercut creates an air gap between the Ge layer and the substrate, severely limiting thermal conduction out from the nanowire and resulting in the destruction of devices under optical pump powers of $\sim 5 \text{ mW}$. To address this limitation, we make use of capillary forces to pull the Ge nanowire down and bring it into contact with the SiO_2 layer when drying the device after the undercut step. The nanowire is then held in contact with the SiO_2 layer by van der Waals forces. The SiO_2 layer enables optical confinement in the Ge while also serving as an additional heat conduction path, permitting a $> 10\times$ increase in pump power. Thermal conduction simulation results are included in the SI (figure S2). Figure 2a,b present height-maps of several devices, gathered using white-light interferometry. Figure 2c presents a line-scan across the single device indicated in Figure 2b. A depression of $\sim 25 \text{ nm}$ can be seen in the vicinity of each device, equal to the thickness of the sacrificial Al_2O_3 layer. Finally, the reattached Ge nanowire is coated with a thin ($\sim 10 \text{ nm}$) conformal Al_2O_3 layer using atomic layer deposition (ALD), passivating the surface and further improving thermal characteristics. Figure 2d presents a side-view schematic of the final device.

Using a combination of finite difference time domain (FDTD) optical simulations (Figure 3a) and finite element method (FEM) mechanical modeling (Figure 3b), we designed a device that supports optical modes with radiative quality factors of over 10^4 while retaining very high ($> 2\%$) mechanical strain along the nanowire. The straight $8 \mu\text{m}$ long $\times 700 \text{ nm}$ wide active region is expanded to a maximum width of $13.7 \mu\text{m}$ and then connected to $20 \mu\text{m}$ wide side pads. The total distance between mirrors is $\sim 30 \mu\text{m}$. 10-period DBR mirrors with a period of 380 nm and a nominal duty cycle of 21% are matched to the shape of the optical mode. Due to the small dimensions of the nanowire, the structure supports no higher-order transverse modes. We provide additional details about the mirror design in the SI.

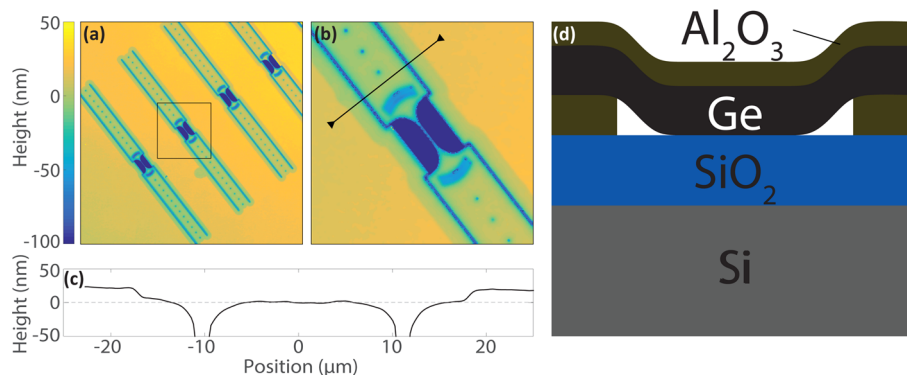


Figure 2. Substrate stiction. (a) Wide-area and (b) detailed height-maps of the wafer surface, gathered using white-light interferometry. The boxed area from a is shown in b. The devices and nearby undercut regions are lower than the wafer surface. Height values below -100 nm are clamped for clarity. (c) Line-scan of the region in b, showing a step height of $\sim 25 \text{ nm}$ at the edge of the undercut region, corresponding to the thickness of the sacrificial Al_2O_3 layer. (d) Side-view schematic of the final material stack. Layer thicknesses are 20 nm Al_2O_3 , 200 nm Ge, 25 nm Al_2O_3 , 850 nm SiO_2 , Si substrate.

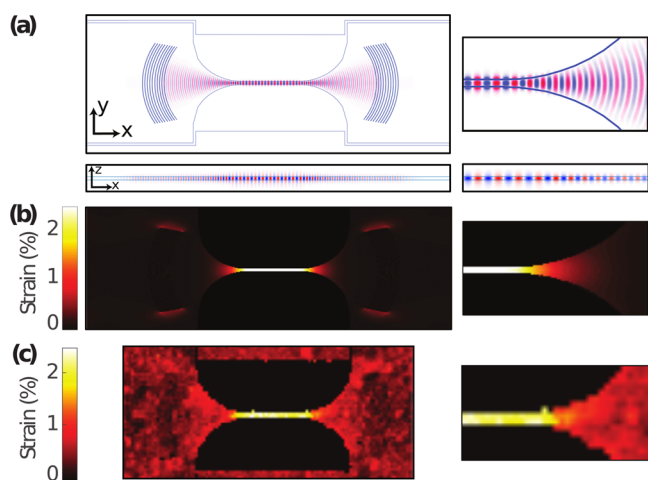


Figure 3. Optical mode and strain distribution. Insets on right show a magnified view of the right side of the wire and adjacent tapered region. (a) E_y field distribution for the optical mode with a free-space wavelength of $2.0 \mu\text{m}$, obtained with FDTD simulation. (b) Tensile strain distribution in an identical structure, obtained with FEM simulation. A uniform strain of $\sim 2.4\%$ is present along the narrow central segment of the nanowire. (c) Strain map for a fabricated device, experimentally obtained using Raman spectroscopy.

From simulations, we find that the strain is very uniform along the straight central region of the nanowire as well as in the out-of-plane direction throughout the device. We calculate an optical confinement factor of 0.37 in the maximally strained region for the mode pictured in Figure 3a. Figure 3c shows an experimentally measured strain distribution in a fabricated device, collected using Raman spectroscopy (details in SI). The result matches our FEM simulations and reveals uniform highly

strained Ge along the length of the nanowire. Additionally, because tensile strain reduces the bandgap of Ge, the spatial variation in the strain profile creates a pseudoheterostructure which confines carriers to the nanowire region, greatly improving carrier concentrations in the gain medium.²⁸

Figure 4a shows photoluminescence spectra from unstrained, 1.95%, and 2.37% strained nanowires with identical optical cavities. The devices were pumped with 2.5 mW of power from a continuous-wave (CW) 980 nm diode laser. The emission peak can be seen to redshift from $\sim 1560 \text{ nm}$ to at least 1980 nm as the strain in the nanowire increases and the bandgap narrows.¹⁶ The position of the emission peak for the 2.37% strained nanowire artificially appears at a shorter wavelength than expected ($>2000 \text{ nm}$) due to a gradual reduction in signal intensity caused by the detection limit of the extended InGaAs photodiode array used to collect the spectra. Optical resonances with a free spectral range of 24.6 nm are visible in the strained wire spectra but are obscured by noise in the unstrained wire spectrum due to low signal intensity. Figure 4b presents a Lorentzian fit to a single optical mode under identical pump conditions. A Q-factor of 2020 is observed, limited by sidewall roughness along the nanowire and material absorption.

Figure 4c presents spectra from a 1.95% strained nanowire under pulsed excitation with various average powers. The pulsed pumping source was a 1550 nm laser with $2 \mu\text{s}$ pulse period and 200 ns pulse length, chosen to minimize heating. Figure 4d displays a series of spectra taken with varying pump powers, with the intensity in each row normalized to its maximum value. Resonances at all wavelengths are seen to shift to shorter wavelengths and broaden as the pump power is increased; both effects are readily explained by increased free carrier densities in the active region. Contrary to previous

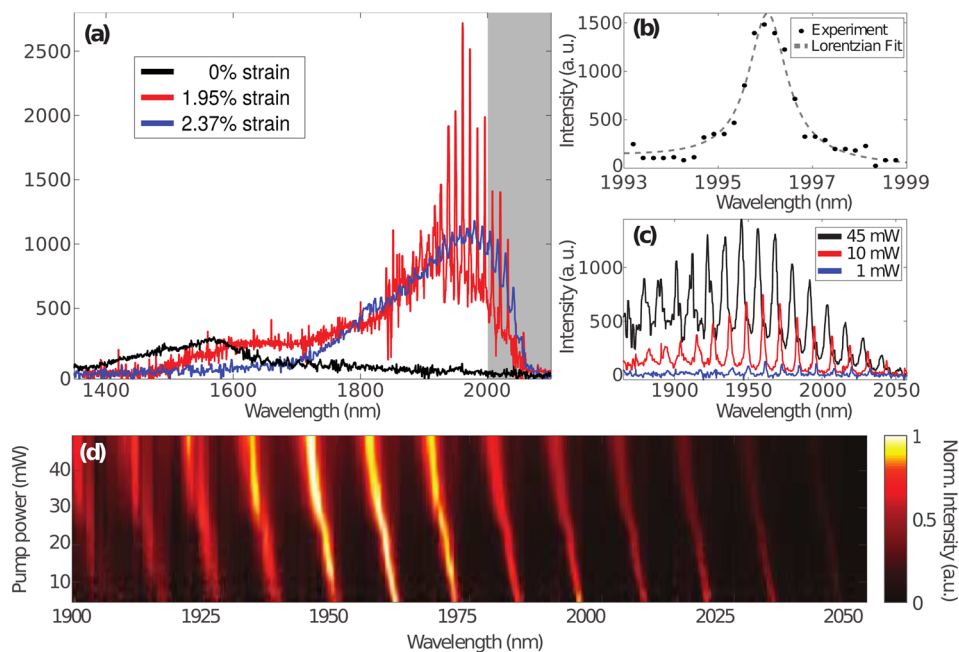


Figure 4. Photoluminescence (PL). (a) PL spectra for devices with 0%, 1.95%, and 2.37% tensile strain. The direct-gap emission intensity increases greatly at higher strain and exhibits high-Q resonances with a free spectral range of 24.6 nm. The detection limit of the spectrometer is denoted with a gray background. (b) Lorentzian fit to a single resonance peak with fitted quality factor of 2020. (c) High resolution PL spectra for a 1.95% strained nanowire pumped with increasing average power from a pulsed laser source. Results at wavelengths below $\sim 1950 \text{ nm}$ include atmospheric absorption lines. (d) Spectral dependence of the emission on the pump power. Each spectrum (row) is normalized to its peak value. A large free-carrier-induced blue shift and significant broadening are observed for all modes.

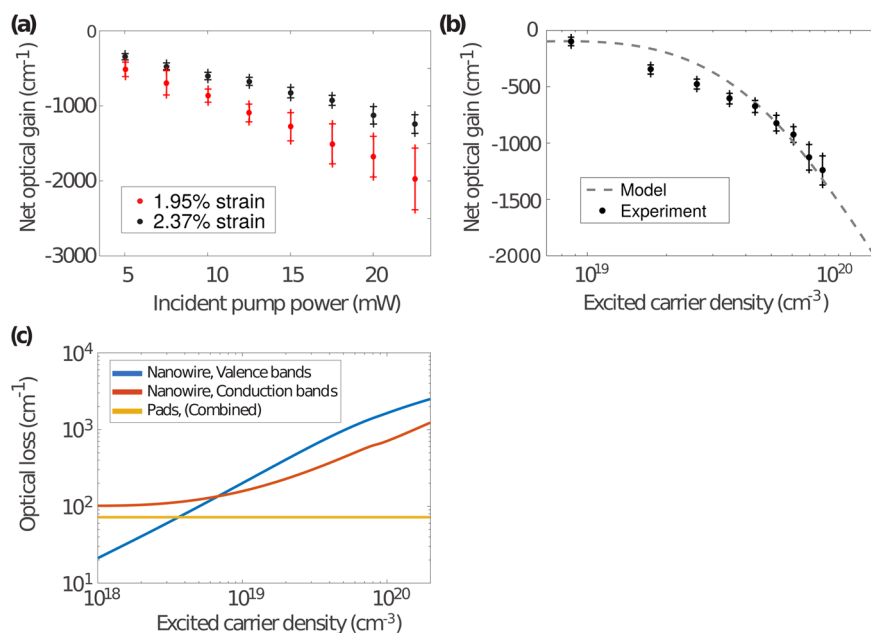


Figure 5. Analysis of net optical gain. (a) Plot of net optical gain versus incident pump power (980 nm CW) for 2.37% (black, $\lambda = 2010$ nm) and 1.95% (red, $\lambda = 1961$ nm) strained nanowires. A clear improvement in net gain is seen in the more strained device. (b) Net optical gain versus injected carrier density for the 2.37% strained device. Black dots indicate experimental data, and the dashed gray line indicates values from EPM calculations. Carrier densities are obtained through calculation of the absorbed laser power and a fit to theory; calculation details are presented in the SI. (c) Plot of optical losses included in the curve presented in b. Losses from valence-band transitions in the highly strained nanowire dominate. At high pump powers, the contribution from the pad regions is negligible due to strong carrier confinement in the pseudoheterostructure.

reports,^{8,9} we did not observe signs of lasing, such as line width narrowing, although our material is highly strained and has a similar doping level to the reported optically pumped Ge-on-Si laser. We estimate that radiative optical losses under 5 mW pump power are 2 \times lower than the net material loss in the nanowire (10 \times lower at 20 mW). As gross material loss is likely significantly higher, we expect that any further increases in radiative Q-factor would be detrimental to the slope efficiency of a strained Ge laser, which is optimal when radiative and gross material losses are similar in magnitude.

To understand the gain/loss mechanisms in our highly strained Ge resonator, we quantitatively calculate the change in net material gain necessary to cause the Q reduction we observe experimentally. We express the net loss $\alpha = (\omega^{1/2}/c)\{[1 + (\sigma_{\text{eff}}/\epsilon\omega)^2]^{1/2}\}^{1/2}$, in terms of the material dielectric constant ϵ , the angular frequency of the emitted light ω , and an effective conductivity σ_{eff} .³⁰ We then relate σ_{eff} to the pump-dependent quality factor $Q_{\text{abs}} = \omega E/P_{\text{abs}}$, where E is the energy in the resonator and P_{abs} is the instantaneous absorbed power. P_{abs} is expressed as $P_{\text{abs}} = \iint_{\text{wire}} \sigma_{\text{eff}} |\mathcal{E}|^2 dV$, where \mathcal{E} is the electric field distribution; self-consistent values of \mathcal{E} and E were taken from FDTD simulation. Finally, we find Q_{abs} by decomposing the experimentally measured quality factor Q_{exp} into two components, a constant cold-cavity quality factor Q_{cold} and a power-dependent component Q_{abs} , with $Q_{\text{exp}}^{-1} = Q_{\text{cold}}^{-1} + Q_{\text{abs}}^{-1}$ and assuming $Q_{\text{abs}} \propto P_{\text{pump}}^{-1}$ (SI, Figure S4).

We plot the net optical gain for 2.37% ($\lambda = 2010$ nm) and 1.95% ($\lambda = 1923$ nm) strained nanowires in Figure 5a. The net gain is seen to decrease with increasing pump power, indicating that increasing free-carrier losses overwhelm any optical gain from the direct-band transition. Nevertheless, we find a significant improvement in net gain as the strain is increased from 1.95% to 2.37%, likely due to an increase in the available optical gain.

To model the net gain present in our structures, we first use the empirical pseudopotential method (EPM) to evaluate the band structure of strained Ge. EPM is known to capture the effects of strain on band structure, including the valence band splitting, particularly well.³¹ Once the band structure of strained Ge is found, it is used to calculate the joint density of states (JDOS) and momentum matrix elements (MME) for band-to-band transitions. Having calculated the JDOS and MME, the absorption (or gain) coefficient for direct transitions between any two bands can be computed using the Fermi's Golden Rule as a function of carrier injection. The transitions considered in this model are the transitions between conduction and valence bands (i.e., the gain), between the valence bands (intervalence-band absorption), and within the conduction band. By fitting this model (Figure 5b, dashed line) to our calculated experimental net gain, we extract a minority carrier lifetime of 2.9 ns, in good agreement with previous measurements.³²

To clarify the dominant loss mechanisms in our modeling, we present them individually in Figure 5c. From this plot, we attribute the Q reduction we observe in our structure primarily to transitions between the valence bands. This is supported by the pump-induced absorption reported by Carroll et al.,¹³ though it is contradictory to existing reports of lasing in Ge.^{8,9}

By increasing strain from 1.95% to 2.37%, we observed a significant reduction in net optical loss, in agreement with the predictions of our model. Extension of our model to higher strain values suggests that net positive gain can be achieved in $\sim 4\%$ strained Ge at room temperature for a doping of 1×10^{19} cm⁻³ and carrier injection of approximately 2×10^{19} cm⁻³. This is a consequence of complex valence band splitting in the very high strain regime, and details of the modeling results will be published elsewhere. As strain values in excess of 5% have been observed experimentally,²⁹ we expect that extension of this

work to devices capable of sustaining 4% or higher tensile strain will enable low-threshold room temperature lasing in Ge.

In summary, we demonstrated greatly enhanced direct-bandgap light emission from a nanowire-based optical resonator. Our device lays the groundwork for a practical group IV nanolaser by integrating high tensile strain, a pseudoheterostructure, and a low-loss optical cavity. We presented resonances with Q factors of up to 2000 and emission tunable over a >400 nm range in devices fabricated with a single lithography step. By performing a quantitative analysis of the pump-dependent net optical gain in our resonators, we found reduced net optical loss from our highly strained devices. At the strain levels achieved in our devices, we determined that losses from valence band transitions dominate any optical gain in our material. We found good agreement between measured net optical gain and EPM modeling, and extracted a minority carrier lifetime of 2.9 ns. We expect that application of further mechanical strain^{16,18} or translation of our work to a GeSn material system¹⁹ will enable practical Si-compatible lasers with order-of-magnitude improvements in threshold over the state of the art.

■ ASSOCIATED CONTENT

● Supporting Information

The Supporting Information is available free of charge on the ACS Publications website at DOI: 10.1021/acs.nanolett.5b03976.

Material stack fabrication process, presents thermal simulations, and provides detailed descriptions of the cavity Q and carrier density calculations; also, the DBR mirror design specifications and Raman spectroscopy methods (PDF)

■ AUTHOR INFORMATION

Corresponding Authors

*E-mail: jela@stanford.edu.

*E-mail: saraswat@stanford.edu.

*E-mail: dwnam@inha.ac.kr.

Author Contributions

J.P. and D.N. contributed equally to this work.

Notes

The authors declare no competing financial interest.

■ ACKNOWLEDGMENTS

We gratefully acknowledge financial support from the AFOSR MURI on Robust and Complex On-Chip Nanophotonics (Dr. Gernot Pomrenke, Grant No. A9550-09-1-0704) and from APIC Corporation (Dr. Raj Dutt). This research was also supported by the Basic Science Research Program through the National Research Foundation of Korea (NRF) funded by the Ministry of Science, ICT & Future Planning (2015R1C1A1A01053117). This work was also supported by an Inha University Research Grant and by the Pioneer Research Center Program through the National Research Foundation of Korea (NRF) funded by the Ministry of Science, ICT & Future Planning (2014M3C1A3052580). J. P. was supported in part by the National Physical Science Consortium Fellowship with stipend support from the National Security Agency. A.Y.P. acknowledges support from the Stanford Graduate Fellowship.

■ REFERENCES

- (1) Miller, D. *Proc. IEEE* **2000**, *88*, 728–749.
- (2) Zhou, Z.; Yin, B.; Michel, J. *Light: Sci. Appl.* **2015**, *4*, e358.
- (3) Liang, D.; Bowers, J. E. *Nat. Photonics* **2010**, *4*, 511–517.
- (4) Chaisakul, P.; Marris-Morini, D.; Frigerio, J.; Chrastina, D.; Roufied, M.-S.; Cecchi, S.; Crozat, P.; Isella, G.; Vivien, L. *Nat. Photonics* **2014**, *8*, 482–488.
- (5) Cho, C.-H.; Aspetti, C. O.; Park, J.; Agarwal, R. *Nat. Photonics* **2013**, *7*, 285–289.
- (6) Takahashi, Y.; Inui, Y.; Chihara, M.; Asano, T.; Terawaki, R.; Noda, S. *Nature* **2013**, *498*, 470–474.
- (7) Rong, H.; Jones, R.; Liu, A.; Cohen, O.; Hak, D.; Fang, A.; Paniccia, M. *Nature* **2005**, *433*, 725–728.
- (8) Camacho-Aguilera, R. E.; Cai, Y.; Patel, N.; Bessette, J. T.; Romagnoli, M.; Kimerling, L. C.; Michel, J. *Opt. Express* **2012**, *20*, 11316–11320.
- (9) Liu, J.; Sun, X.; Camacho-Aguilera, R.; Kimerling, L. C.; Michel, J. *Opt. Lett.* **2010**, *35*, 679–681.
- (10) Wirths, S.; Geiger, R.; von den Driesch, N.; Mussler, G.; Stoica, T.; Mantl, S.; Ikonik, Z.; Luysberg, M.; Chiussi, S.; Hartmann, J. M.; Sigg, H.; Faist, J.; Buca, D.; Grutzmacher, D. *Nat. Photonics* **2015**, *9*, 88–92.
- (11) Koerner, R.; Oehme, M.; Gollhofer, M.; Schmid, M.; Kostecki, K.; Bechler, S.; Widmann, D.; Kasper, E.; Schulze, J. *Opt. Express* **2015**, *23*, 14815–14822.
- (12) Liu, J.; Sun, X.; Pan, D.; Wang, X.; Kimerling, L. C.; Koch, T. L.; Michel, J. *Opt. Express* **2007**, *15*, 11272–11277.
- (13) Carroll, L.; Friedli, P.; Neuenschwander, S.; Sigg, H.; Cecchi, S.; Isa, F.; Chrastina, D.; Isella, G.; Fedoryshyn, Y.; Faist, J. *Phys. Rev. Lett.* **2012**, *109*, 057402.
- (14) Boucaud, P.; El Kurdi, M.; Ghrib, A.; Prost, M.; de Kersauson, M.; Sauvage, S.; Aniel, F.; Checoury, X.; Beaudoin, G.; Largeau, L.; Sagnes, I.; Ndong, G.; Chaigneau, M.; Ossikovski, R. *Photonics Res.* **2013**, *1*, 102–109.
- (15) Nam, D.; Sukhdeo, D.; Roy, A.; Balram, K.; Cheng, S.-L.; Huang, K. C.-Y.; Yuan, Z.; Brongersma, M.; Nishi, Y.; Miller, D.; Saraswat, K. *Opt. Express* **2011**, *19*, 25866–25872.
- (16) Nam, D.; Sukhdeo, D.; Gupta, S.; Kang, J.-H.; Brongersma, M.; Saraswat, K. *IEEE J. Sel. Top. Quantum Electron.* **2014**, *20*, 16–22.
- (17) Capellini, G.; Reich, C.; Guha, S.; Yamamoto, Y.; Lisker, M.; Virgilio, M.; Ghrib, A.; El Kurdi, M. E.; Boucaud, P.; Tillack, B.; Schroeder, T. *Opt. Express* **2014**, *22*, 399–410.
- (18) Dutt, B.; Sukhdeo, D.; Nam, D.; Vulovic, B.; Yuan, Z.; Saraswat, K. *IEEE Photonics J.* **2012**, *4*, 2002–2009.
- (19) Sukhdeo, D. S.; Saraswat, K. C.; Dutt, B. R.; Nam, D. *arXiv:1506.08402*.
- (20) Suess, M. J.; Geiger, R.; Minamisawa, R. A.; Schiefler, G.; Frigerio, J.; Chrastina, D.; Isella, G.; Spolenak, R.; Faist, J.; Sigg, H. *Nat. Photonics* **2013**, *7*, 466–472.
- (21) Ghrib, A.; El Kurdi, M.; de Kersauson, M.; Prost, M.; Sauvage, S.; Checoury, X.; Beaudoin, G.; Sagnes, I.; Boucaud, P. *Appl. Phys. Lett.* **2013**, *102*, 221112.10.1063/1.4809832
- (22) Sanchez-Perez, J. R.; Boztug, C.; Chen, F.; Sudradjat, F. F.; Paskiewicz, D. M.; Jacobson, R.; Lagally, M. G.; Paiella, R. *Proc. Natl. Acad. Sci. U. S. A.* **2011**, *108*, 18893–18898.
- (23) Prost, M.; El Kurdi, M.; Ghrib, A.; Sauvage, S.; Checoury, X.; Zerounian, N.; Aniel, F.; Beaudoin, G.; Sagnes, I.; Boeuf, F.; Boucaud, P. *Opt. Express* **2015**, *23*, 6722–6730.
- (24) Al-Attili, A. Z.; Kako, S.; Husain, M.; Gardes, F.; Higashitarumizu, N.; Iwamoto, S.; Arakawa, Y.; Ishikawa, Y.; Arimoto, H.; Oda, K.; Ido, T.; Saito, S. *Front. Mater.* **2015**, *2*, 10.3389/fmats.2015.00043
- (25) Sun, G.; Soref, R. A.; Cheng, H. H. *J. Appl. Phys.* **2010**, *108*, 033107.10.1063/1.3467766
- (26) Chen, R.; Gupta, S.; Huang, Y.-C.; Huo, Y.; Rudy, C. W.; Sanchez, E.; Kim, Y.; Kamins, T. I.; Saraswat, K. C.; Harris, J. S. *Nano Lett.* **2014**, *14*, 37–43.
- (27) Minamisawa, R. A.; Süess, M. J.; Spolenak, R.; Faist, J.; David, C.; Gobrecht, J.; Bourdelle, K. K.; Sigg, H. *Nat. Commun.* **2012**, *3*, 1096.

- (28) Nam, D.; Sukhdeo, D. S.; Kang, J.-H.; Petykiewicz, J.; Lee, J. H.; Jung, W. S.; Vučković, J.; Brongersma, M. L.; Saraswat, K. C. *Nano Lett.* **2013**, *13*, 3118–3123.
- (29) Sukhdeo, D. S.; Nam, D.; Kang, J.-H.; Brongersma, M. L.; Saraswat, K. C. *Photonics Res.* **2014**, *2*, A8–A13.
- (30) Jackson, J. D. *Classical Electrodynamics*; Wiley: New York, 1962; p 224.
- (31) Fischetti, M. V.; Laux, S. E. *J. Appl. Phys.* **1996**, *80*, 2234–2252.
- (32) Nam, D.; Kang, J.-H.; Brongersma, M. L.; Saraswat, K. C. *Opt. Lett.* **2014**, *39*, 6205–6208.